This paper was presented at the 16th Wind Integration Workshop, 25-27 October 2017, and published in the workshop's proceedings.

Frequency Support from OWPPs connected to HVDC via Diode Rectifiers

Oscar Saborío-Romano, Ali Bidadfar, Ömer Göksu, Nicolaos A. Cutululis

Department of Wind Energy
Technical University of Denmark
Risø Campus, Denmark
Email: osro@dtu.dk

***Abstract*—This paper presents a study assessing the actual capability of an offshore wind power plant (offshore WPPs, OWPPs) to provide frequency support (FS) to an onshore network, when connected through a high-voltage direct-current (HVDC) link having a diode rectifier (DR) offshore terminal and a voltage source converter (VSC) onshore terminal. Both primary and fast frequency response (PFR and FFR, respectively) are studied, and both the power reserves from preventive curtailment and the kinetic energy stored in the rotating masses of the wind turbines (WTs) are considered as sources of additional power during onshore under-frequency events. Three methods are considered for overloading the WTs, including the proposed External Reference method, in which the base active power reference can be set externally. The performance of the controls is studied by means of electromagnetic transient (EMT) simulations, for which an aggregated model of the OWPP is used. The results suggest that such OWPPs can in principle provide onshore FS by means of plant-level active power control strategies already developed for OWPPs connected to HVDC via VSCs. Some of the results also suggest that it may be unnecessary to overload the WTs if active power reserves from curtailed operation are available when providing both PFR and FFR.**

***Index Terms*—HVDC, offshore wind power plant, diode rectifier, frequency support**

I. Introduction

Networks linking the offshore wind power plants (offshore WPPs, OWPPs) and the onshore networks in different countries are needed to fully exploit Europe's offshore wind resources. Most of the currently installed OWPPs make use of the traditional high-voltage alternating-current (HVAC) technology to export their production to the onshore networks, and only a few are connected through high-voltage direct-current (HVDC) links based on voltage source converters (VSCs). OWPPs connected through HVDC are, however, widely expected to proliferate, as the distance from shore increases and the costs associated to the power converter technology decrease.

Diode rectifiers (DRs) have been recently proposed as a viable alternative for connecting OWPPs comprised of type-4 (full-converter) wind turbines (WTs) to HVDC networks, reducing costs and increasing reliability [1]–[5]. Since such offshore HVDC terminals are inherently devoid of the controllability of VSCs, their use relies on transferring the corresponding control responsibilities to the WT front-end (FE) VSCs. Fundamentally different WT and WPP controls are therefore required i.e., their control philosophy has to be changed from that of grid-following units to that of grid-forming units [3], [4], [6].

The current technical connection requirements for HVDC-linked offshore generation are based on a paradigm having controllable grid-forming HVDC offshore terminals (e.g., VSCs), which is innately incompatible with passive, uncontrollable terminals such as DRs. However, before requirements specific for OWPPs connected via DRs can be established, more comprehensive studies are needed, to asses the actual capabilities of such solutions to contribute to the secure operation of the networks that will be connected to them [6]–[9].

The main objective of the present study is to asses the actual capability of an OWPP to provide frequency support (FS) to an onshore alternating-current (AC) network, when connected through a HVDC link having a DR offshore terminal and a VSC onshore terminal [9]. The study also aims at examining the compatibility of corresponding higher-level controls previously devised for VSC-HVDC-connected OWPPs [10], [11]. Through such controls, the OWPP modifies its active power output according to the onshore frequency signal directly communicated to it.

Two kinds of frequency response are considered: primary frequency response (PFR) and fast frequency response (FFR). The PFR is based on an active-power-frequency droop, with the reserves from preventively curtailed operation considered as the source of additional active power during onshore under-frequency events. Based on the rate of change of the frequency deviation, the FFR is meant to contribute to the stabilisation of the onshore AC networks during the first stage of large frequency excursions. The kinetic energy stored in the rotating masses of the WT rotor and drive train systems is considered as the main source of additional power for such response during onshore under-frequency events [10], [12], [13].

While similar studies conducted for VSC-HVDC-connected OWPPs have focused on either the PFR or the FFR, drawing on either the reserves from curtailment or the stored kinetic energy [10], [11], [14], this study considers both kinds of frequency response and both sources of additional active power during onshore under-frequency events. Moreover, a method has been proposed for overloading the WTs, as an alternative to those available in the literature [11], [15].

The rest of the paper is organised as follows. In Section II, the investigated system is described, the main control algorithms are detailed, and the three different WT overloading methods are explained. In Section III, some of the considered

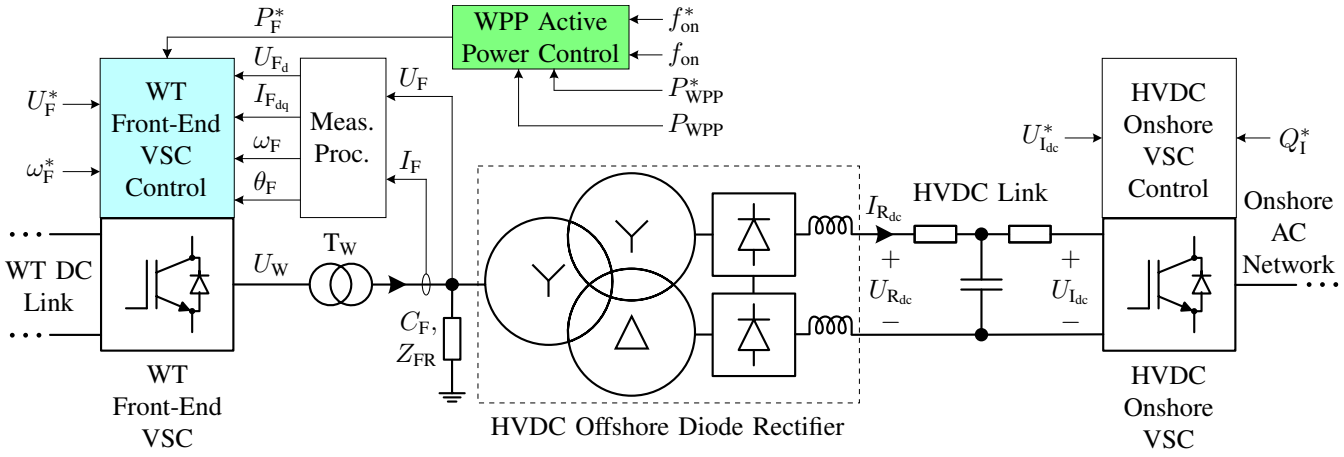

Figure 1: Overview of the investigated system and control structure

cases are described, and corresponding simulation results are presented and discussed. Finally, concluding remarks are made in Section IV, and considerations for future work are outlined in Section V.

II. Modelling and Control

Figure 1 shows an overview of the investigated system and of the associated control structure. The system is comprised of an OWPP connected to an onshore AC network by means of a monopolar HVDC link and is based on those studied in [2], [4], [5]. Balanced/symmetric operation is assumed.

The WPP is modelled as an aggregated type-4 (full-converter) WT. Its DC link dynamics are not considered, and the corresponding voltage is thus assumed constant (ideally regulated). The front-end VSC injects the WT/WPP output active power, P_F, into the offshore AC network through the WT step-up transformer, $\mathrm{T_W}$, with leakage inductance L_W.

The HVDC offshore terminal is modelled as a diode-based (uncontrolled) 12-pulse rectifier (diode rectifier, DR), with corresponding reactive power compensation, C_F, and filter bank, Z_FR, on its AC side. The submarine cables connecting the HVDC terminals are modelled using the equivalent T circuit. The HVDC onshore terminal consists of a VSC, which controls the voltage on its DC terminals, $U_{\mathrm{I_{dc}}}$, and the reactive power injected to the onshore AC network, Q_I.

The onshore AC network is modelled as a lumped three-phase synchronous machine (SM) with its governor and turbine, and a three-phase load. The wind power penetration is $25\,\%$ (i.e., the WPP is rated at $400\,\mathrm{MW}$, in a $1600\,\mathrm{MW}$ system). The onshore frequency, f_on, is calculated from the AC voltage measured at the HVDC onshore terminal's point of connection with the onshore AC network and is transmitted directly to the OWPP. No communication delay is considered.

Switching effects and any delay due to the implementation of the pulse-width modulation (PWM) are neglected, and ideal average models are used for the power electronic converters. Moreover, the PWM is assumed to be done in the linear range, and the VSC filter dynamics are not considered.

A. WT Front-End VSC Control

The WT front-end VSC control, shown in Figure 2, is based on those described in [2], [4], [5]. It is implemented on a rotating reference frame (RRF) oriented on the voltage at the point of connection, U_F, i.e., $U_{\mathrm{F_d}} = U_\mathrm{F}$, $U_{\mathrm{F_q}} = 0$. The inner current control loops, shown in the right side of Figure 2, are comprised of proportional-integral (PI) controllers with decoupling terms and forward feeding of the measured $U_{\mathrm{F_d}}$. The outer control loops, shown in the left side of Figure 2, are based on the dynamics of C_F and include forward feeding of the measured active and reactive currents, $I_{\mathrm{F_d}}$ and $I_{\mathrm{F_q}}$, respectively. The offshore frequency control is implemented by means of a proportional regulator manipulating $I_{\mathrm{F_q}}$.

When the DR is not conducting, the WT/WPP operates in voltage control mode, in which a PI regulator controls U_F by means of $I_{\mathrm{F_d}}$. By having the HVDC onshore VSC control $U_{\mathrm{I_{dc}}}$ and increasing the (offshore AC) voltage reference, U_F^*, to a high enough value e.g., $1.1\,\mathrm{p.u.}$, the DR starts conducting and acts as a voltage clamp on U_F i.e., it no longer follows U_F^*, as it is determined by $U_{\mathrm{I_{dc}}}$ and the HVDC rectifier current, $I_{\mathrm{R_{dc}}}$. The output of the voltage control: the active current reference, $I_{\mathrm{F_d}}^*$, reaches then its maximum value, $I_{\mathrm{F_{d,max}}}^*$, and the WPP/WT operates in current control mode. In this mode, P_F is controlled by manipulating $I_{\mathrm{F_{d,max}}}^*$, which indirectly limits $I_{\mathrm{R_{dc}}}$. A voltage-dependent current order limiter (VDCOL) is used to protect the WT/WPP while allowing it to ride through faults.

B. WPP Active Power Control

To study the capability of the WT/WPP to provide FS to the onshore AC network, the model is extended to include the supervisory active power control at plant level, shown in Figure 3, based on the controllers proposed in [10], [11] for OWPPs connected to HVDC via VSCs. In the right side of Figure 3, a PI regulator controls the WPP active power output, P_WPP, which is—in the studied system—equal to P_F. A first-order low-pass filter (LPF) is applied to the corresponding measurement signal. Physical and control limits are modelled by means of corresponding restrictions on the regulator's output value and its rate of change. P_WPP can be controlled to follow the WPP active power reference, P_WPP^*, which is normally equal to or lower than the aerodynamic power available from the wind, $P_\mathrm{ava}(v)$, i.e., $P^* = P_\mathrm{WPP}^* \leq P_\mathrm{ava}(v)$.

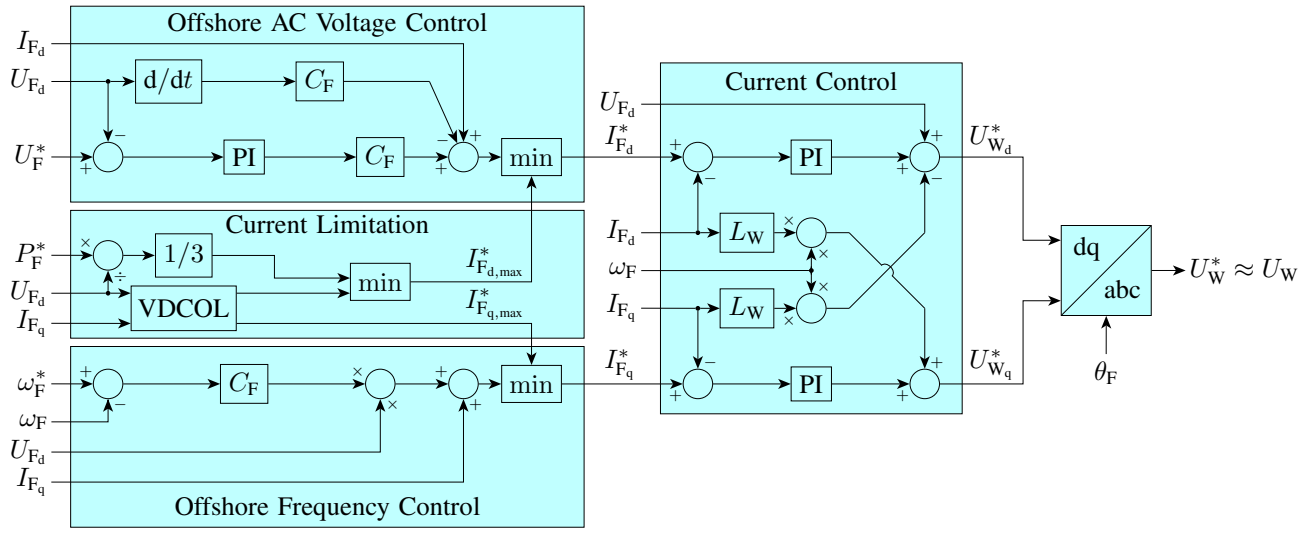

Figure 2: Wind turbine front-end voltage source converter control

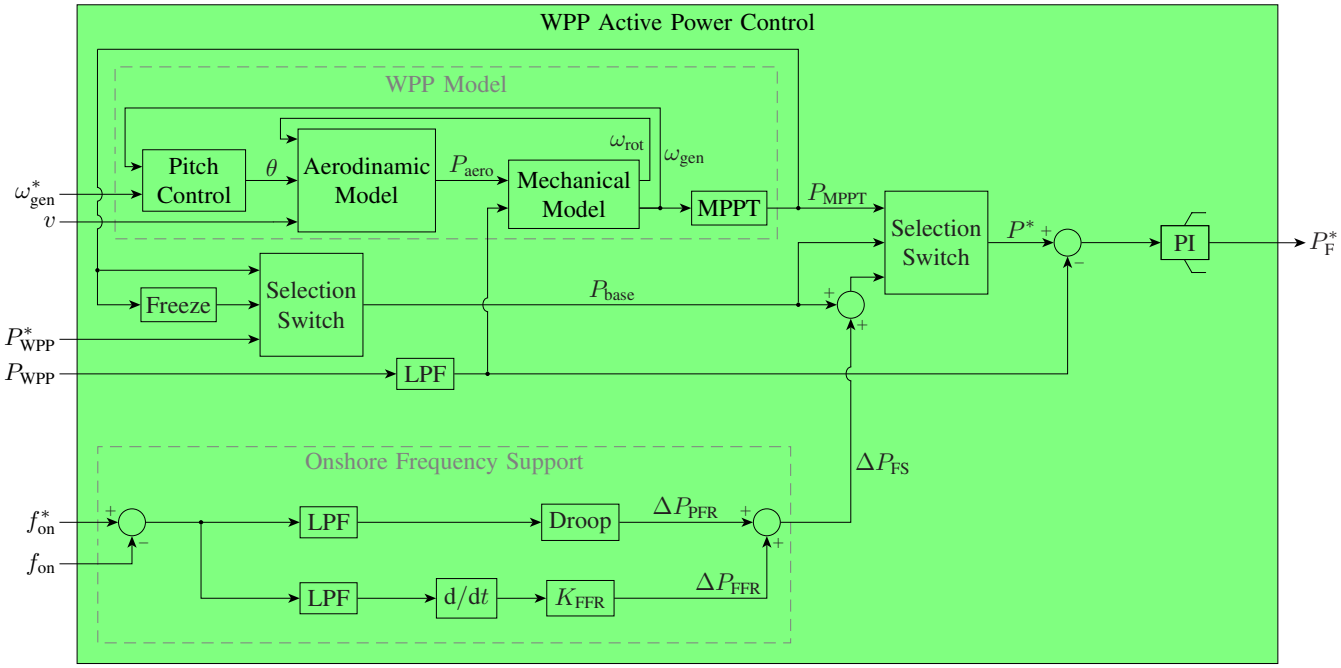

Figure 3: Wind power plant active power control

An internal aggregated model of the WPP, shown in the top-left area of Figure 3, is included to represent the WT rotor dynamics relevant to the study of FS from WPPs and the overloading of the WTs. It is based on those used in [11], [16], [17] and consists mainly of an aerodynamic model, a mechanical model, a pitch control model and a maximum power point tracking (MPPT) look-up table.

1) Normal Production: If the WPP is not required to curtail its production, its WTs follow their normal production characteristic (MPPT curve) i.e., $P^* = P_{\text{MPPT}}(\omega_{\text{gen}})$. While operating on such curve, the WT aerodynamic efficiency is optimal for wind speeds lower than the nominal one, $v < 1\,\text{p.u.}$, the pitch control is inactive and the WTs operate at a constant zero pitch angle, $\theta = 0$. For higher wind speeds, the WTs run at rated power, and the pitch controller keeps the WT generator rotational speed, ω_{gen}, at its nominal value [16] i.e., $P_{\text{MPPT}}(\omega_{\text{gen}} = \omega^*_{\text{gen}} = 1\,\text{p.u.}) = 1\,\text{p.u.}$

2) Curtailed Production: When the WPP curtails its production, $P^* = P^*_{\text{WPP}} < P_{\text{aero}} = P_{\text{ava}}(v)$, the power imbalance, $P_{\text{aero}} > P_{\text{WPP}}$, causes the WT rotors to accelerate until ω_{gen} reaches $1\,\text{p.u.}$ To maintain $\omega_{\text{gen}} = 1\,\text{p.u.}$, the pitch control then increases θ (i.e., pitches the WT blades), which decreases the aerodynamic/mechanical power, P_{aero}, until power balance is restored, $P_{\text{aero}} = P_{\text{WPP}} < P_{\text{MPPT}} = 1\,\text{p.u.}$

3) Onshore Frequency Support: To provide FS to the onshore AC network, the base active power reference, P_{base}, is modified, as shown at the bottom of Figure 3, by means of an additional active power reference, ΔP_{FS}, based on the onshore frequency, f_{on}, which is communicated continuously to the WPP i.e., $P^* = P_{\text{base}} + \Delta P_{\text{FS}}(f_{\text{on}})$. PFR is implemented by including in ΔP_{FS} a component, ΔP_{PFR}, proportional to the deviation of f_{on} from its nominal/reference value, $f^*_{\text{on}} = 1\,\text{p.u.}$, calculated using a given (piecewise-defined) droop characteristic. Moreover, a component, ΔP_{FFR}, pro-

portional to the rate of change of such deviation, $\mathrm{d}f_{\text{on}}/\mathrm{d}t$, is added to provide FFR.

4) WT Overloading: In order to extract kinetic energy from their rotating masses, WTs are overloaded when providing FFR during onshore under-frequency events. During overloading, $P^* = P_{\text{base}} + \Delta P_{\text{FS}} > P_{\text{aero}} \leq P_{\text{ava}}(v)$, the power imbalance, $P_{\text{aero}} < P_{\text{WPP}}$, causes the WT rotors to decelerate (ω_{gen} decreases), which results in P_{MPPT} also decreasing. After releasing the overloading, the WTs are allowed to recover their speed by operating on the MPPT curve, $P^* = P_{\text{MPPT}} \leq P_{\text{aero}}$, until $P_{\text{WPP}} = P_{\text{aero}} = P_{\text{base}} + \Delta P_{\text{FS}}$.

Three WT overloading methods are considered, based on three different approaches to setting P_{base} during overloading (inputs to the selection switch in the left side of Figure 3). In the External MPPT method, P_{base} is fixed at the (frozen) value of P_{MPPT} just before the start of the overloading [11], [15], $P_{\text{base}} = P_{\text{MPPT}_0}$, whereas in the proposed External Reference method it is set externally, $P_{\text{base}} = P^*_{\text{WPP}}$. By using the latter, P_{base} can be set to a different value e.g., a value of less than $P_{\text{MPPT}_0} = 1\,\text{p.u.}$ in the case of preventively curtailed production. In the Internal method, the WT dynamics are considered during overloading by having $P_{\text{base}} = P_{\text{MPPT}}$, resulting in a smaller decrease in P_{WPP} after releasing the overloading [11], [15].

III. Simulation Results

Results of the performed electromagnetic transient (EMT) simulations are presented in Figure 4 and Figure 5. The OWPP production is curtailed preventively to provide active power reserves of 10 %, so that initially, $P_{\text{WPP}} = P_{\text{ava}}(v) - 0.1\,\text{p.u.} \Rightarrow \omega_{\text{gen}} = 1\,\text{p.u.} = P_{\text{MPPT}}$ (see Section II-B2). Frequency events are simulated by means of $\pm 15\,\%$ load step changes (i.e., $\pm 240\,\text{MW}/16\,000\,\text{MW}$) at $t = 0.5\,\text{s}$. The average wind speed, v, is considered constant during each simulation. Each figure includes base case responses, corresponding to no FS from the WPP to the onshore AC network (i.e., the frequency response consisting solely of that of the SM). The grey and red signals in each figure represent the base case, CBase, and the case with the OWPP providing PFR only, CP, respectively. As can be seen in Figure 4 and Figure 5, the frequency response can be improved by having the OWPP provide FS to the onshore AC network.

The WPP response to an onshore over-frequency event at low wind speed is shown in Figure 4. The curves in black represent the addition of FFR to the FS, CPF. Since no additional power is needed, the WTs are not overloaded. By decreasing P_{WPP}, the WPP's PFR reduces f_{on} and maintains it at a lower value for as long as the wind allows, as depicted in CP. However, the decrease in P_{WPP} is restricted by the minimum production limit, $P_{\text{WPP}} \geq 2.5\,\%$, imposed by the non-linear properties of the DR [13]. In reaction to the corresponding increase in ω_{gen}, the pitch control pitches the WTs so as to maintain ω_{gen} at 1 p.u.

The addition of the FFR improves the onshore FS further by reducing the rate of change of frequency (ROCOF) just after the event, also reducing the frequency zenith as a consequence, as illustrated in CPF. Nevertheless, the constraints imposed on the rate of change of the WT active power references, $-0.1\,\text{p.u.}/\text{s} \leq \mathrm{d}P^*_{\text{F}}/\mathrm{d}t \leq 0.1\,\text{p.u.}/\text{s}$, limit the speed

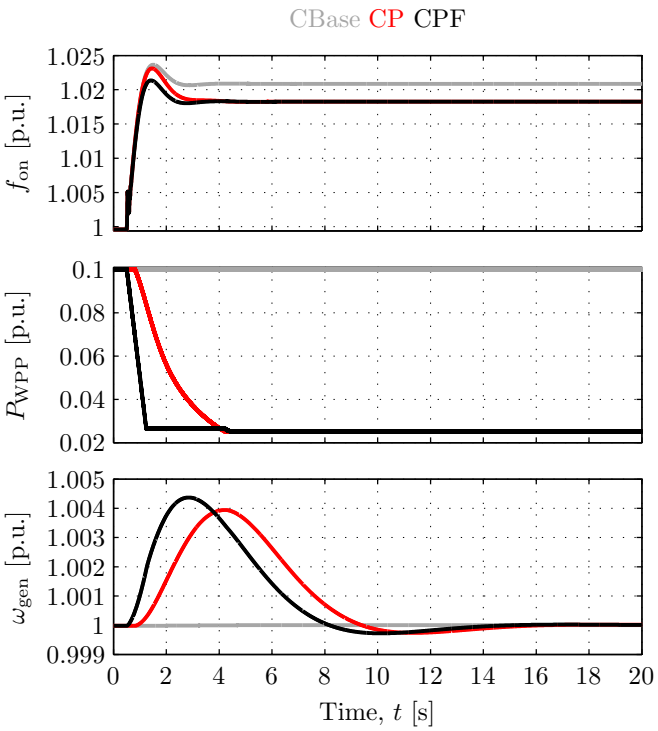

Figure 4: WPP's response to an onshore over-frequency event at low wind speed – CBase: $P^* = P^*_{\text{WPP}}$, CP: $P^* = P^*_{\text{WPP}} + \Delta P_{\text{PFR}}$, CPF: $P^* = P^*_{\text{WPP}} + \Delta P_{\text{FS}}$

of such response and thus the corresponding improvement in the onshore FS. To further improve the frequency response, the restriction $\mathrm{d}P^*_{\text{F}}/\mathrm{d}t \leq 0$ is briefly applied following the frequency zenith, on which $\Delta P_{\text{FFR}}(\mathrm{d}f_{\text{on}}/\mathrm{d}t)$ changes sign.

Figure 5 illustrates the response of the WPP to an onshore under-frequency event at high wind speed. The three last sets of curves depict the addition of FFR to the FS, overloading the WTs with a different method in each case (see Section II-B4). The overloading is released at $t = 13\,\text{s}$. The Internal method is used in the case represented by the blue signals, CPFI, whereas the yellow and green curves correspond to the cases in which the External Reference, CPFE-ref, and External MPPT, CPFE-MPPT, methods are applied, respectively.

Drawing on the active power reserves, the WPP's PFR increases f_{on} by increasing P_{WPP} and maintains it at a higher value for as long as the wind allows, as illustrated in CP. As depicted in CPFE-ref, the addition of the FFR improves the onshore FS further by reducing the ROCOF just after the event, also reducing the frequency nadir as a consequence. However, the speed of such response and corresponding improvement in the onshore FS is limited by the restrictions imposed on $\mathrm{d}P^*_{\text{F}}/\mathrm{d}t$, as in CPF in Figure 4. To further improve the frequency response, the constraint $\mathrm{d}P^*_{\text{F}}/\mathrm{d}t \geq 0$ is briefly applied following the frequency nadir, on which $\Delta P_{\text{FFR}}(\mathrm{d}f_{\text{on}}/\mathrm{d}t)$ changes sign. As opposed to CPFE-MPPT and CPFI, the lower value given in this case to the base power reference, $P_{\text{base}} = P^*_{\text{WPP}} = 0.9\,\text{p.u.}$ produces no overloading of the WTs (i.e., the active power reserves suffice for the provision of both PFR and FFR).

If P_{base} is set to a high enough value (e.g., 1 p.u.), the WTs are overloaded and the WPP produces more than

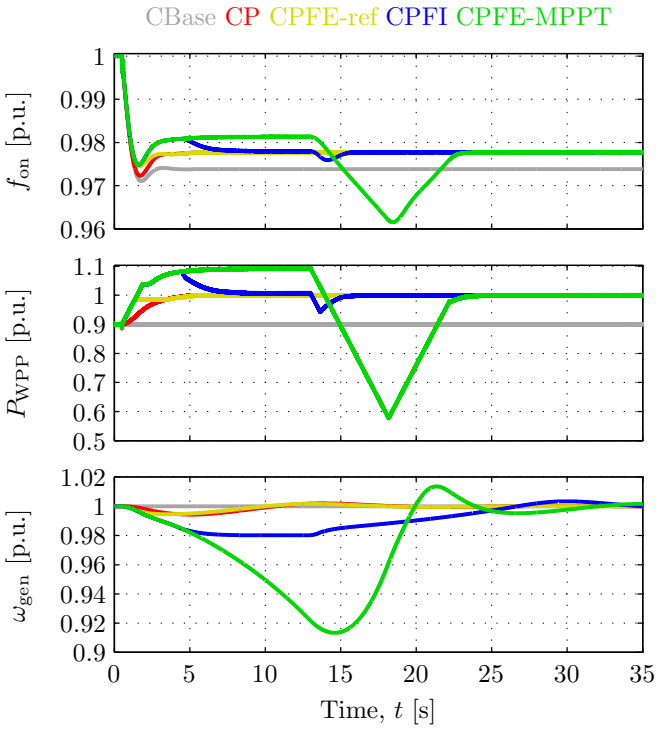

Figure 5: WPP's response to an onshore under-frequency event at high wind speed – CBase: $P^* = P^*_{\text{WPP}}$, CP: $P^* = P^*_{\text{WPP}} + \Delta P_{\text{PFR}}$, CPFE-ref: $P^* = P^*_{\text{WPP}} + \Delta P_{\text{FS}}$, CPFI: $P^* = P_{\text{MPPT}} + \Delta P_{\text{FS}}$, CPFE-MPPT: $P^* = P_{\text{MPPT}_0} + \Delta P_{\text{FS}}$

the available aerodynamic power, $P_{\text{ava}}(v) = 1\,\text{p.u.}$, at the expense of a reduction in ω_{gen}, as shown in CPFE-MPPT and CPFI. This results in a further reduction of the ROCOF just after the event and thus of the nadir. Such reduction is, however, also limited by the restrictions imposed on $\mathrm{d}P^*_{\text{F}}/\mathrm{d}t$, making such and any further improvement to the onshore FS smaller.

Fixing the value of P_{base} at $P_{\text{MPPT}_0} = 1\,\text{p.u.}$ in CPFE-MPPT results in an overproduction of at least $5\,\%$ for about $10\,\text{s}$, until the overloading is released. As a consequence, f_{on} is increased and maintained at a value higher than in CP and CPFE-ref. When the overloading is released, P_{WPP} and f_{on} are reduced as the WTs recover their speed, producing a new under-frequency event with a nadir much greater than the original one in CBase. Moreover, the constraints imposed on $\mathrm{d}P^*_{\text{F}}/\mathrm{d}t$ worsen the new event by extending its duration. If, however, the Internal method is used for overloading the WTs, as in CPFI, P_{WPP} follows the reduction in $P_{\text{MPPT}}(\omega_{\text{gen}})$ during the overloading and reaches $P_{\text{ava}}(v) = 1\,\text{p.u.}$ within a few seconds. Such reduction in the overproduction period results in a shorter recovery (underproduction) period (after releasing the overloading) with much smaller reductions in P_{WPP} and f_{on}.

IV. Conclusions

The simulation results suggest that OWPPs connected to HVDC via DRs can in principle provide FS to onshore AC networks by means of plant-level active power control strategies already developed for OWPPs connected to HVDC via VSCs. Employing such strategies, the OWPPs can provide PFR during an onshore frequency events, reducing the frequency deviation and maintaining it at a lower value for as long as the wind allows. Moreover, preventively operating OWPPs constantly curtailed can provide the additional active power needed for providing such response during onshore under-frequency events. The minimum production limit (e.g., $2.5\,\%$), imposed by the non-linear properties of the DRs, may, nevertheless, restrict such capability during onshore over-frequency events at low wind speeds.

The OWPPs can improve the onshore FS by also providing FFR, reducing the ROCOF just after the frequency event, also reducing the frequency nadir/zenith further as a consequence. Such improvement, however, will be limited by the constraints imposed on the active power references dispatched to the WTs, P^*_{F}. In the proposed External Reference method for overloading the WTs, the base active power reference can be set externally e.g., to a value different than those in the other two overloading methods. By overloading their WTs, the OWPPs can also provide more than the available aerodynamic power (overproduce) for several seconds during an onshore under-frequency event, as has been illustrated for high wind speed conditions. This, nonetheless, can result in a—possibly worse—new onshore frequency event during the recovery (underproduction) period. Moreover, it may even be unnecessary if active power reserves from curtailed operation are available, as such reserves may suffice for the provision of both PFR and FFR.

V. Future Work

Communication delays will be considered in future related studies, and the models will be extended to include several (aggregated) WPPs/WTs/WT strings.

VI. Acknowledgement

This work has received funding from the European Union's Horizon 2020 research and innovation programme under grant agreement No 691714.

References

[1] R. M. Blasco-Giménez, S. C. Añó-Villalba, J. Rodríguez-D'Derlée, R. S. Peña-Guiñez, R. Cárdenas-Dobson, S. I. Bernal-Pérez, and F. Morant-Anglada, "Fault Analysis of Uncontrolled Rectifier HVDC Links for the Connection of Off-shore Wind Farms", in *Proceedings of the IEEE Industrial Electronics Society 35th Annual Conference (IECON 2009)*, Porto, Portugal, 3rd–5th Nov. 2009, pp. 468–473.

[2] R. M. Blasco-Giménez, S. C. Añó-Villalba, J. Rodríguez-D'Derlée, S. I. Bernal-Pérez, and F. Morant-Anglada, "Diode-Based HVdc Link for the Connection of Large Offshore Wind Farms", *IEEE Transactions on Energy Conversion*, vol. 26, no. 2, pp. 615–626, Mar. 2011.

[3] T. Christ, S. Seman, and R. Zurowski, "Investigation of DC Converter Nonlinear Interaction with Offshore Wind Power Park System", in *Proceedings of the 2015 EWEA Offshore Conference*, Copenhagen, Denmark, 10th–12th Mar. 2015.

[4] S. I. Bernal-Pérez, "Integración híbrida multipunto en el sistema eléctrico de grandes parques eólicos marinos a través de redes de alta tensión en continua", PhD thesis, Technical University of Valencia, Valencia, Spain, Nov. 2015.

[5] S. I. Bernal-Pérez, S. C. Añó-Villalba, and R. M. Blasco-Giménez, "Stability Analysis of HVDC-Diode Rectifier Connected Off-shore Wind Power Plants", in *Proceedings of the IEEE Industrial Electronics Society 41st Annual Conference (IECON 2015)*, Yokohama, Japan, 9th–12th Nov. 2015, pp. 4040–4045.

[6] O. Saborío-Romano, A. Bidadfar, Ö. Göksu, M. Altin, N. A. Cutululis, and P. E. Sørensen, "Connection of OWPPs to HVDC networks using VSCs and Diode Rectifiers: An Overview", in *Proceedings of the 15th Wind Integration Workshop*, Vienna, Austria, 15th–17th Nov. 2016.

[7] ENTSO-E, "Network Code on HVDC Connections (HVDC)", Brussels, Belgium, Network Code, Oct. 2015. [Online]. Available: https://www.entsoe.eu/major-projects/network-code-development/high-voltage-direct-current/Pages/default.aspx.

[8] ——, "Network Code on Requirements for Grid Connection Applicable to all Generators (RfG)", Brussels, Belgium, Network Code, Apr. 2016. [Online]. Available: https://www.entsoe.eu/major-projects/network-code-development/requirements-for-generators/Pages/default.aspx.

[9] PROMOTioN, "Deliverable 3.1: Detailed functional requirements to WPPs", Project Deliverable, Jan. 2017. [Online]. Available: https://www.promotion-offshore.net/fileadmin/PDFs/D3.1_PROMOTioN_Deliverable_3.1_Detailed_functional_requirements_to_WPPs.pdf.

[10] L. Zeni, "Power system integration of VSC-HVDC connected wind power plants, Control principles, power system services, clustering of wind power plants", PhD thesis, Technical University of Denmark, Roskilde, Denmark, Mar. 2015.

[11] J. N. Sakamuri, A. D. Hansen, N. A. Cutululis, M. Altin, J. Sau-Bassols, E. Prieto-Araujo, and O. Gomis-Bellmunt, "Suitable Method of Overloading for Fast Primary Frequency Control from Offshore Wind Power Plants in Multi-Terminal DC Grid", in *Proceedings of the IEEE PowerTech Manchester 2017 Conference*, Manchester, United Kingdom, 18th–22nd Jun. 2017.

[12] G. C. Tarnowski, "Coordinated Frequency Control of Wind Turbines in Power Systems with High Wind Power Penetration", PhD thesis, Technical University of Denmark, Roskilde, Denmark, Nov. 2011.

[13] PROMOTioN, "Deliverable 3.2: Specifications of the control strategies and the simulation test cases", Project Deliverable, Mar. 2017. [Online]. Available: https://www.promotion-offshore.net/fileadmin/PDFs/D3.2_Specifications_Control_strategies_and_simulation_test_cases.pdf.

[14] L. Zeni, A. J. Rudolph, J. Münster-Swendsen, I. Margaris, A. D. Hansen, and P. Sørensen, "Virtual inertia for variable speed wind turbines", *Wind Energy*, vol. 16, no. 8, pp. 1225–1239, Nov. 2013.

[15] S. Wachtel, and A. Beekmann, "Contribution of Wind Energy Converters with Inertia Emulation to frequency control and frequency stability in power systems", in *Proceedings of the 8th Wind Integration Workshop*, Bremen, Germany, 14th–15th Oct. 2009.

[16] A. D. Hansen, M. Altin, I. D. Margaris, F. Iov, and G. C. Tarnowski, "Analysis of the short-term overproduction capability of variable speed wind turbines", *Renewable Energy*, vol. 68, no. 1, pp. 326–336, Aug. 2014.

[17] G. Rousi, "Methods for representations of wind farms in dynamic power system studies", Master's thesis, Technical University of Denmark, Roskilde, Denmark, Nov. 2013.